Physics of Plasmas

RESEARCH ARTICLE | MARCH 27 2024

On discriminating tokamak sawtooth crash models via localized density and temperature measurements

D. Liu ; W. Fox ; S. Bose ; H. Ji ; S. Jardin ; N. Ferraro

Phys. Plasmas 31, 032512 (2024)
https://doi.org/10.1063/5.0186504

On discriminating tokamak sawtooth crash models via localized density and temperature measurements

Cite as: Phys. Plasmas **31**, 032512 (2024); doi: 10.1063/5.0186504
Submitted: 6 November 2023 · Accepted: 22 February 2024 ·
Published Online: 27 March 2024

D. Liu,[1,a)] W. Fox,[1,2,b)] S. Bose,[2] H. Ji,[1,2] S. Jardin,[2] and N. Ferraro[2]

AFFILIATIONS

[1]Princeton University, Princeton, New Jersey 08540, USA
[2]Princeton Plasma Physics Laboratory, Princeton, New Jersey 08540, USA

[a)]Electronic mail: dingyunl@princeton.edu
[b)]Author to whom correspondence should be addressed: wfox@pppl.gov

ABSTRACT

The core electron temperature drops rapidly during the sawtooth crash in tokamak plasmas, which causes heat loss and may lead to fast particle losses or even a disruption. Several models have been proposed for the periodic crash, including the Kadomtsev model with magnetic reconnection and the quasi-interchange model with the growth of higher-mode-number pressure-driven instabilities. 3D MHD simulations were performed for these two models with a goal to develop intuition and to predict qualitatively how different types of sawtooth will appear in various diagnostics. The structures of electron density n_e and electron temperature T_e show a dominant (1, 1) mode for the Kadomtsev case and a dominant (4, 4) mode for the quasi-interchange case. The oscillations of n_e and T_e have a positive correlation near the inversion layer for both cases, while their frequencies and amplitudes are different depending on the dominant modes. Particularly, for the Kadomtsev case, we find a relation between the amount of flux reconnected during a sawtooth event and n_e or T_e oscillations. Therefore, we connect recently developed measurement capabilities for n_e and T_e to the internal sawtooth behavior. We propose that this method of analysis can help in identifying the type of sawtooth in future experiments augmented by simulations.

I. INTRODUCTION

The sawtooth oscillation is a phenomenon commonly found in tokamaks characterized by regular periodic reorganization of the core plasma.[1] During each cycle, the core electron density and temperature first gradually ramp up and then drop rapidly, with the signals in the shape of a sawtooth. This dramatic crash may excite other modes, such as the neoclassical tearing mode (NTM), and eventually lead to disruptions.[2]

A major issue of the sawtooth study is what causes such a fast crash. Different models have been proposed to address this problem. Kadomtsev attributes it to resistive magnetic reconnection.[3] In this model, the centrally peaked toroidal current density leads to higher temperature in the center by Ohmic heating, where the plasma becomes less collisional and more conductive. Hence, the toroidal current density peaks even more strongly. When the central safety factor q_0 drops sufficiently, the plasma becomes subject to a $(m, n) = (1, 1)$ resistive kink instability. The magnetic field is reconnected, leading to a flattening of the temperature inside the $q = 1$ surface, and q_0 returns to 1. This model successfully explains the cyclic evolution for initial q_0 significantly below unity, yet the resistive reconnection timescale is too slow compared to laboratory observations.[4] Within this reconnection picture, mechanisms, such as two-fluid effects[5] and the plasmoid instability,[6] have been proposed from simulations to enable fast reconnection and a fast temperature drop. Alternatively, Wesson[7] developed a model with the pressure-driven ideal MHD mode. The plasma becomes unstable to an ideal MHD (1, 1) interchange mode when q_0 is slightly above unity, and the density and temperature profiles are flattened out on an ideal MHD timescale, which is driven by interchange instabilities. Later, Jardin *et al.*[8] extended this model, pointing out that in scenarios with peaked pressure and low magnetic shear, the ideal MHD (1, 1) interchange mode saturates at a low amplitude and produces a central loop voltage through the dynamo effect that keeps $q_0 \geq 1$.[9] It is then other unstable interchange modes (m, n) with $m = n > 1$ that trigger the crash.

The lack of direct diagnostics has limited experimental studies of sawteeth. While dedicated laboratory experiments, such as the

Magnetic Reconnection eXperiment (MRX),[10] can directly measure the reconnection rate as well as obtain full in-plane measurements of electric and magnetic fields, and plasma density and temperature, this type of measurement has been difficult in tokamaks. Different q profiles give rise to different sawtooth models; however, the interpretation of motional Stark effect (MSE) measurements of the q profile before the crash occurs differs widely among groups.[11–14] Our goal is to advance internal diagnostics to improve understanding of the sawtooth crash. For example, concrete measurements for localized T_e have been provided by electron cyclotron emission imaging (ECEI) on tokamaks,[15–17] and more recently, fast n_e measurements localized to the $q = 1$ surface have also been enabled by beam emission spectroscopy (BES).[18]

In this study, we run two different sawtooth simulations with comparable parameters using the 3D MHD code M3D-C1.[19] Previously, this code has been used for several studies of sawtooth dynamics, including the role of two fluids effects[20] and stochasticity[21,22] within reconnection models. Additionally, it revealed the quasi-interchange scenarios.[8] With representative M3D-C1 simulation data, we aim to develop diagnostic predictions for two different sawtooth models, namely, Kadomtsev-type sawteeth with reconnection compared to quasi-interchange sawteeth. The main control parameter is the initial q profile. In case 1, q_0 begins at 0.83, while in case 2, the profile is flat in the center, and q_0 is close to unity. Case 1 is observed to be dominated by a strong resistive (1, 1) mode, leading to a kink out of the core and formation of a long thin current sheet during the crash and reconnection, following a Kadomstev-reconnection-type picture. In contrast, case 2 lies in the "quasi-interchange" scenario of Jardin *et al.*[8] It is dominated by a (4, 4) helical mode, and no single dominant current sheet is formed during the crash. The overall goal of the study is to develop intuition and diagnostic predictions to compare between the two sawtooth models, keeping as many quantities in the profiles as similar as possible.

The hallmark of both BES and ECEI is that they make observations at fixed spatial points or a fixed poloidal plane for imaging, additionally complicated by the strong toroidal rotation of the plasma. Accordingly, we analyze how rotating plasmas with these helical perturbations will appear on such fixed diagnostics. For both cases, we observe that the helical modes produce toroidal oscillations in a rotating plasma. We focus attention near the inversion layer, which is defined as the minor radius r_{inv} such that $\delta T_e < 0$ for $r < r_{inv}$ and $\delta T_e > 0$ for $r > r_{inv}$, i.e., $\delta T_e = 0$ at $r = r_{inv}$. That is, the inversion layer is the point where T_e apparently does not change during the sawtooth crash. We find that, near the inversion layer, the n_e and T_e oscillations are initially in phase and peak at the crash. The oscillations have only one period in each toroidal rotation for case 1 and four for case 2. This difference can be utilized to distinguish the two types of sawtooth in future experiments. We find that n_e oscillation up to 10% and T_e oscillation up to 20% or 40% are predicted to occur, which is qualitatively comparable to recent measurements.[18,23] Finally, for the Kadomtsev case with reconnection, we draw a relation between the amount of reconnected flux with the oscillations of n_e and T_e at the $q = 1$ surface from their dependence on the plasma core displacement, which may enable BES and ECEI as indirect diagnostics for the reconnection rate.

In Sec. II, we describe the simulation setups of these two cases. In Sec. III, we identify the type of sawtooth event from each simulation case and compare the results with a focus on the 2D poloidal structures. In Sec. IV, we explore more detailed diagnostic signatures of the localized n_e and T_e evolution predicted by the two models. In Sec. V, we draw a connection from n_e and T_e to reconnection in the Kadomtsev case. Finally, in Sec. VI, we summarize the conclusions and discuss the experimental application of the simulation results.

II. SIMULATION SETUPS

We set up two nonlinear 3D MHD simulation cases using the M3D-C1 code.[19,24] The starting point for the simulation setup and equilibrium is from Jardin *et al.*[8] The simulation domain is a D-shape tokamak with major radius of $R = 3.2\,\mathrm{m}$, minor radius of $a = 1.0\,\mathrm{m}$, ellipticity of 1.3, and triangularity of 0.2. The ion species is hydrogen, and all the physical values are dimensionless with the normalization: $l_{norm} = 1.0\,\mathrm{m}$, $n_{norm} = 4 \times 10^{19}\,\mathrm{m}^{-3}$, $B_{norm} = 1.0\,\mathrm{T}$, $v_{norm} = v_A = B_{norm}/\sqrt{\mu_0 n_{norm} m_i} = 3.45 \times 10^6\,\mathrm{m\,s}^{-1}$.

Case 1 makes small modifications to the Jardin *et al.*[8] equilibrium to produce a Kadomtsev-like sawtooth event with a strong (1, 1) resistive kink. Case 2 is initialized identically to the Jardin *et al.*[8] equilibrium. To generate a sawtooth of the Kadmotsev type for a clean comparison, all the input parameters are kept the same apart from the initial profiles of the safety factor q and pressure p. Table I shows the different input parameters used to set up the initial q and p profiles generated by the M3D-C1 Grad–Shafranov solver. `q0` is an M3D-C1 input parameter, which is approximately the initial central safety factor; `p0` is the central pressure, normalized by $p_0 = B_0^2/2\mu_0$, where $B_0 = B_{norm}$; and `p1` and `p2` are parameters of the analytic pressure function. The case simulating the Kadomtsev type starts with the ramp-up phase of the first sawtooth. The initial q_0 is 0.83, and the initial pressure is lower such that $\beta \sim 1\%$. The kink instability dominates over the pressure-driven interchange instabilities to trigger the sawtooth. By contrast, the drastic drop of T_e for the quasi-interchange case happened toward the beginning of the simulation, and we focus on this sawtooth. This case has an initial q_0 very close to 1, and its initial pressure is about three times that of case 1.

A neutral beam is included as a source of particles, energy, and momentum. The resistivity is chosen to be Spitzer-like, $\eta \propto T_e^{-3/2}$, therefore, evolving with the plasma temperature profile; however, it is increased by a factor of 264 over the physical resistivity for numerical stability. Thus, the central Lundquist number S is the order of 10^6 for the quasi-interchange case. Although S is not set as high as physical values, it is high enough to achieve a quasi-interchange type of sawtooth. An isotropic viscosity $\mu = 10^{-5}\mu_{norm}$ is applied, where $\mu_{norm} = n_{norm} m_i l_{norm} v_{norm}$. The thermal conductivity κ is highly anisotropic, as the heat transport parallel to the magnetic field is much larger than the perpendicular transport in the tokamak. Here, we choose the perpendicular component to be proportional to $(n^3/p)^{1/2}$, $\kappa_\perp = 1.75 \times 10^{-6}\kappa_{norm}$, and the parallel component $\kappa_\parallel = 5\kappa_{norm}$, where $\kappa_{norm} = k_B n_{norm} l_{norm} v_{norm}$. The diffusivity D is isotropic, and $D = 10^{-5} D_{norm}$, where $D_{norm} = l_{norm} v_{norm}$. The values of

TABLE I. Input parameters to setup the initial q and p profiles.

Case	Type	`q0`	`p0`	`p1`	`p2`
1	Kadomtsev	0.8	0.01	0	0
2	Quasi-interchange	0.975	0.035	−0.5	0

thermal conductivity and diffusivity are larger than realistic to aid in numerical stability and resolution requirements, and also to cut down the interval between two crashes.

The average edge of an element of the unstructured mesh in the poloidal plane is 0.06 m. A convergence study of the toroidal resolution was done by doubling the number of toroidal planes (36 for the original cases). The two cases display qualitatively the same behaviors in the physical properties of interest. Nonlinear 2D tests are also made to confirm that the transport coefficients are properly chosen and do not alter the evolution qualitatively.

We also spot-checked a few different values of q_0 and p_0 for case 1, and we found that the overall qualitative behavior does not change, though the instability is stronger for lower q_0. We will return to discussing this and other parameters we have scanned in Sec. VI.

III. SAWTOOTH TYPE AND 2D STRUCTURES

The results of the two simulation cases are shown in Figs. 1–6. Figure 1 shows the time series of T_e on the magnetic axis. Both cases start with the ramp-up phase. The temperature gradually increases and crashes abruptly, developing into the sawtooth shape, which has been observed in many tokamak experiments.[25,26] A few time-points are indicated, which correspond to the end of the ramp-up phase, during the crash, and after the crash of each sawtooth event. They are marked by dashed vertical lines with the labels "ramp," "crash," and "post."

Figure 2 shows the flux-averaged n_e, T_e, and q profiles on the midplane at the end of the ramp-up phase and after the sawtooth crash for the two cases. For case 1, n_e and T_e are centrally peaked, and q_0 is significantly below 1 before the crash. After the crash, the profiles of n_e and T_e become flat, and q_0 reverts to 1. For case 2, the q_0 starts from very close to 1. It increases to above 1 during the crash and holds through the end of the crash. Though T_e is obviously flattened out in this case, the relaxation in n_e right after the crash is not as pronounced.

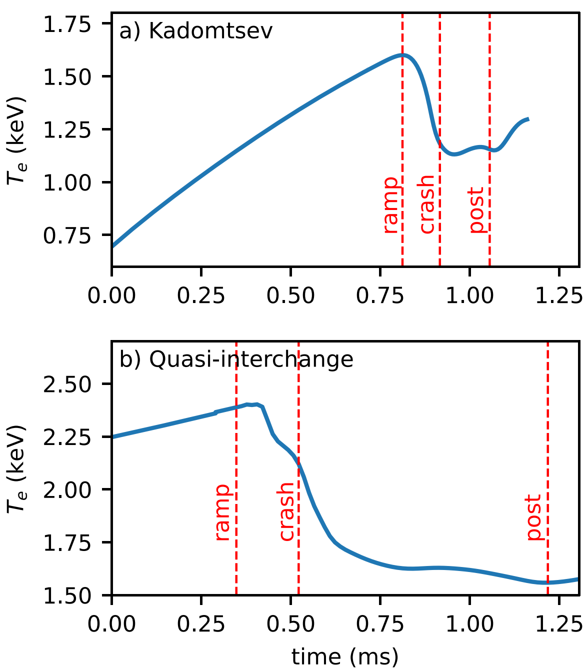

FIG. 1. Time series of T_e on the magnetic axis: (a) case 1, the Kadomtsev type and (b) case 2, the quasi-interchange type. The three dashed vertical lines in each plot indicate the time-points at different stages of each sawtooth event.

Zooming into the crash phase in Fig. 1, the kinetic energy in each of the first nine toroidal harmonics during the crash is shown in Fig. 3. The dashed vertical lines are identical to those in Fig. 1 for each case. The kinetic energy increases on a hybrid resistive/ideal timescale for the Kadomtsev case but on a faster ideal MHD timescale for the quasi-interchange case, indicating different dominant instabilities for the two cases. After growing during the ramp-up phase, the kinetic energy peaks when the crash happens. For the Kadomtsev case, the $n = 1$ mode dominates throughout the whole period. For the quasi-interchange case, the $n = 4$ mode peaks most strongly during the crash, and other high number modes $n = 3, 5$ also become dominant sequentially after the crash. Therefore, we expect to see different structures in n_e and T_e for the two different cases.

Poincaré plots, which track the recurrence of some sample magnetic field lines on a poloidal section, are made to show the magnetic field configuration. Figure 4 displays the Poincaré plots at the featured time-points of each case, except that (f) is taken around 5 ms (later than post). As is shown in the first row for case 1, a (1, 1) island appears near the inversion layer during the ramp-up phase. It gradually grows and expels the plasma core to the outboard side. When the crash happens, the island takes the place of the original core rapidly and forms the new core in (c). We notice that the new core is accompanied by a large region of stochasticity outside the q = 1 surface after the crash in Fig. 5(c). Various tokamak experiments[27,28] have reported that stochasticity is sometimes related to incomplete reconnection of sawtooth events. Therefore, one question is whether the reconnection is complete for this case modeling Kadomtsev sawtooth. In a previous study of incomplete sawtooth at ASDEX Upgrade,[28] the (1, 1) resistive kink mode survives the crash and decays slowly afterward, and q_0 decreases and increases periodically but always remains below unity. By contrast, a KSTAR study validating the "full reconnection model" observed $q_0 < 1.0$ before the crash and $q_0 \geq 1.0$ in the MHD quiescent period after the crash.[29] Our simulation shows that the (1, 1) mode develops and eventually becomes the new core, and q_0 goes above unity after the crash, indicating that the reconnection is complete in the Kadomtsev case.

The evolution of the magnetic field configuration for case 2 illustrated in the second row is very different. The plasma core is first deformed in shape during the ramp-up phase, but there is no obvious change in the topology. Later, islands composed of high-number modes, such as $n = 3, 4, 5$, dominate within the inversion layer. They become unstable abruptly and trigger the crash, causing a stochastic region to form near the magnetic axis. Despite this stochasticity shown in Fig. 4(e), the original core persists through the whole process, and the rational surfaces are restored afterward. Figure 4(f) is taken at a later time than "post" to show the state when the magnetic surfaces are mostly reformed.

The 2D structures of n_e and T_e together with contours of current density parallel to the magnetic field $j_\parallel$ at the featured times are shown in Fig. 5 for case 1 and Fig. 6 for case 2. In case 1, $j_\parallel$ is initially monotonic with the peak near the magnetic axis. As the island grows, $j_\parallel$ begins to drop along the inversion layer, eventually reversing sign and forming a strong current sheet, which indicates the occurrence of magnetic reconnection. A (1, 1) structure is also observed in n_e and T_e with

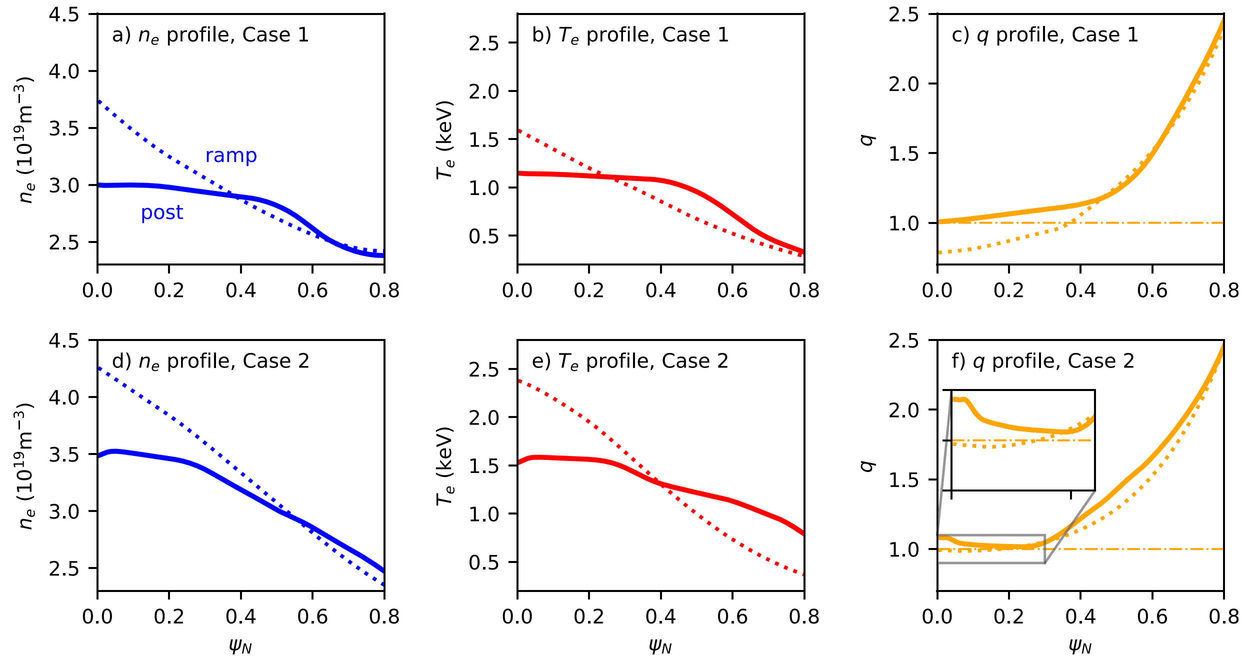

FIG. 2. The flux-averaged n_e (blue), T_e (red), and q (orange) profiles on the midplane for case 1 (the top row) and case 2 (the bottom row). The solid/dotted curves correspond to the times "ramp" and "post."

its peak moving with the original core until it is flattened out at the end of the crash. The behavior is much different for case 2. Figure 6(a) shows that the current perturbations are highly patchy rather than organized into a current sheet. This patchiness results from the overlap of multiple unstable MHD modes. In general, no continuous current sheet appears near the inversion layer during the crash. The dominant (4, 4) structures in n_e and T_e become more defined during the ramp-up phase, but the shapes are complex due to the simultaneous existence of other high-number modes.

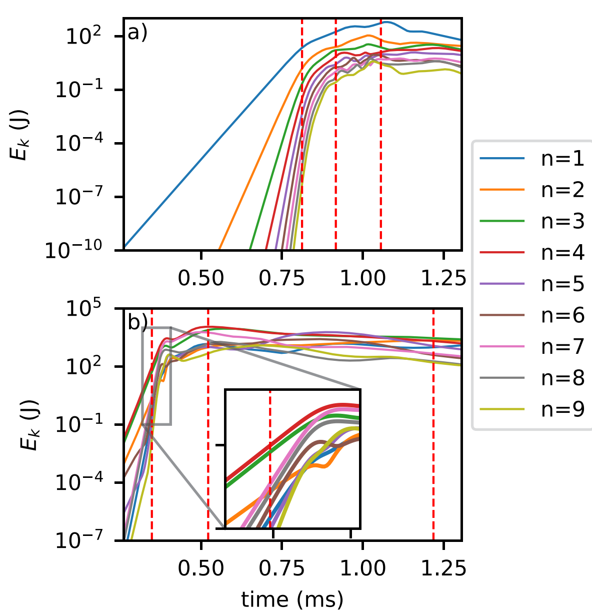

FIG. 3. Zoom-in view of the kinetic energy in each of the first nine toroidal harmonics in the crash phase. (a) Case 1, the Kadomtsev type and (b) case 2, the quasi-interchange type.

IV. LOCALIZED n_e AND T_e EVOLUTION

Tokamak plasmas typically rotate fast toroidally, but the 2D diagnostics are usually fixed to certain toroidal angles in experiments. Simulation complements diagnostic data by providing data in the whole plasma volume. To study the correlation between density and temperature near the inversion layer, n_e and T_e are plotted along the toroidal direction at the inversion point on the midplane. We find $R = 3.7$ m for case 1 and $R = 3.9$ m for case 2. Figure 7 shows the oscillations of n_e and T_e at $(R, Z) = (3.7, 0)$ m along the toroidal direction for case 1. The subplots are arranged in the time sequence, with (a), (c), and (e) corresponding to ramp, crash, and post times and (b) and (d) to time-points in between. We find n_e and T_e only have a single period in each toroidal rotation, corresponding to a (1, 1) island. The amplitude of the oscillations grows during the ramp-up phase, reaching its largest at the crash, and decreasing after the crash. In case 2, as shown by Fig. 8, in contrast there are four periods for both n_e and T_e in (a) and (b), and three periods in (c) and (d), which agrees with the predominant (4, 4) and (3, 3) modes observed in Fig. 3. n_e and T_e stay in phase for both cases, indicating there is a positive correlation of density and temperature. This positive correlation is a consequence of the hot plasma core kinking out, which brings the high n_e and T_e together and then flattens out the peaked profiles of n_e and T_e.

The amplitude of the oscillations is studied by computing the root mean square along the toroidal direction

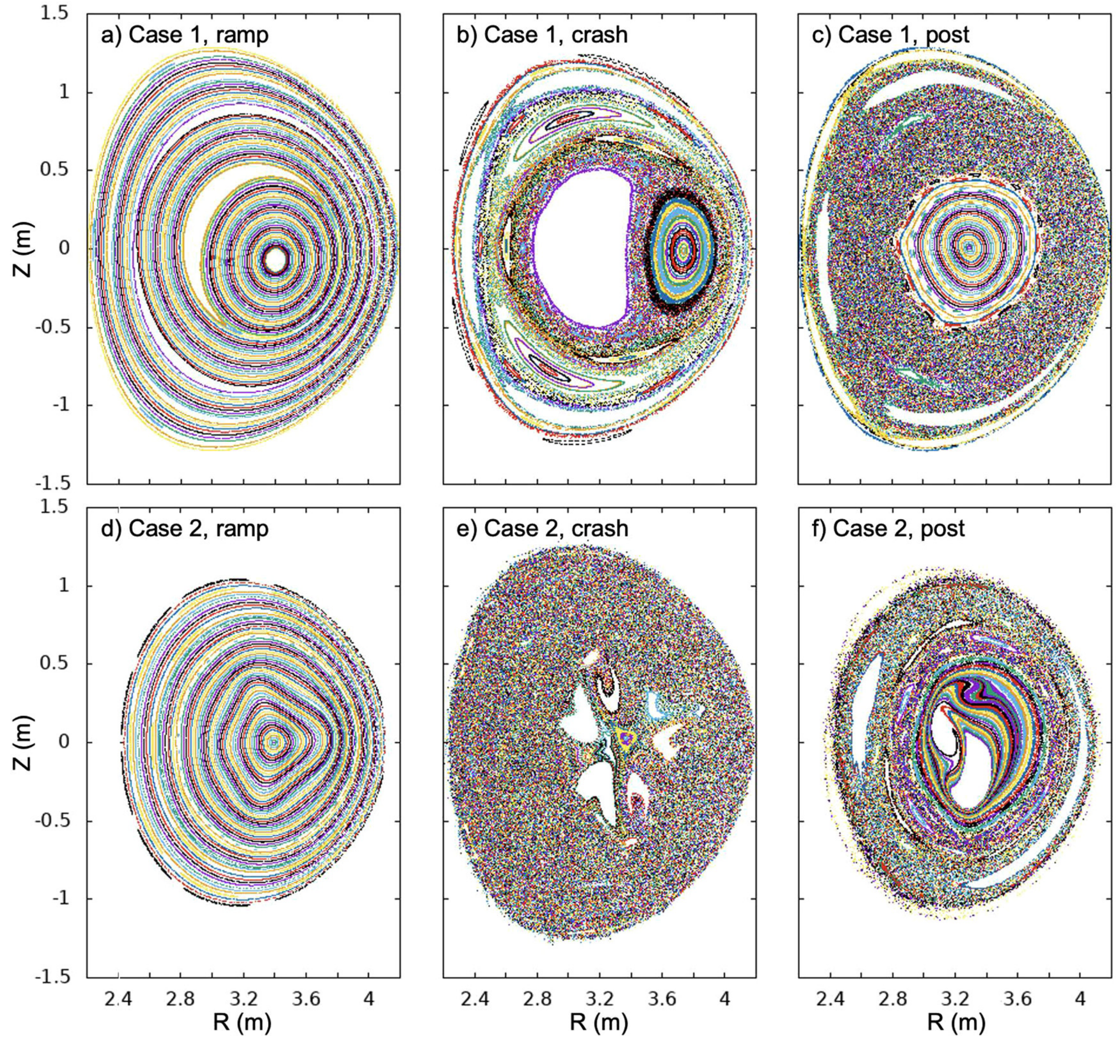

FIG. 4. Poincaré plots showing the magnetic field configuration. (a)–(c) correspond to the times ramp, crash, and post of case 1, the Kadomtsev type and (d)–(f) for those of case 2, the quasi-interchange type.

$$\frac{\langle \delta n_e \rangle}{\langle n_e \rangle} = \frac{1}{\langle n_e \rangle} \sqrt{\frac{1}{2\pi} \int_0^{2\pi} (n_e(\phi) - \langle n_e \rangle)^2 d\phi}, \tag{1a}$$

$$\frac{\langle \delta T_e \rangle}{\langle T_e \rangle} = \frac{1}{\langle T_e \rangle} \sqrt{\frac{1}{2\pi} \int_0^{2\pi} (T_e(\phi) - \langle T_e \rangle)^2 d\phi}, \tag{1b}$$

where $n_e(\phi)$ and $T_e(\phi)$ are taken at toroidal angle ϕ of a fixed poloidal location—$(R, Z) = (3.7, 0)$ m for case 1 and $(3.9, 0)$ m for case 2; and $\langle n_e \rangle$ and $\langle T_e \rangle$ are the toroidal average of $n_e(\phi)$ and $T_e(\phi)$. Figure 9 shows that in both cases, $\langle \delta n_e \rangle / \langle n_e \rangle$ and $\langle \delta T_e \rangle / \langle T_e \rangle$ peak with large amplitude when the crash begins. We also observe that the density fluctuations decay more slowly than the temperature fluctuations in both cases. This is a consequence of fast parallel heat transport. We find $(\langle \delta n_e \rangle / \langle n_e \rangle)_{max} \sim 10\%$ in both cases and $(\langle \delta T_e \rangle / \langle T_e \rangle)_{max} \sim 20\%$ in case 1 and $(\langle \delta T_e \rangle / \langle T_e \rangle)_{max} \sim 40\%$ in case 2. We have done some spot-checks for other values of q_0 for case 1. When the initial q_0 is reduced to $\sim$0.7, $(\langle \delta n_e \rangle / \langle n_e \rangle)_{max}$ does not change obviously, indicating that it is not very sensitive to the initial q_0 in the simulation. But $(\langle \delta T_e \rangle / \langle T_e \rangle)_{max}$ increases to $\sim$30% with this more unstable equilibrium.

V. RELATING n_e AND T_e TO RECONNECTION IN THE KADOMTSEV CASE

It would be valuable to develop indirect diagnostics of the reconnection rate for sawteeth. With localized measurement of n_e and T_e enabled by BES[18] and ECEI, we are motivated to relate n_e and T_e to reconnection.

With further study of the Kadomtsev case, we establish a relation between the n_e and T_e oscillations at the $q = 1$ surface and the amount of magnetic reconnection in the ramp-up phase via their dependence on the MHD perturbation. The MHD perturbation is represented by the displacement of the flux surface ξ, which is

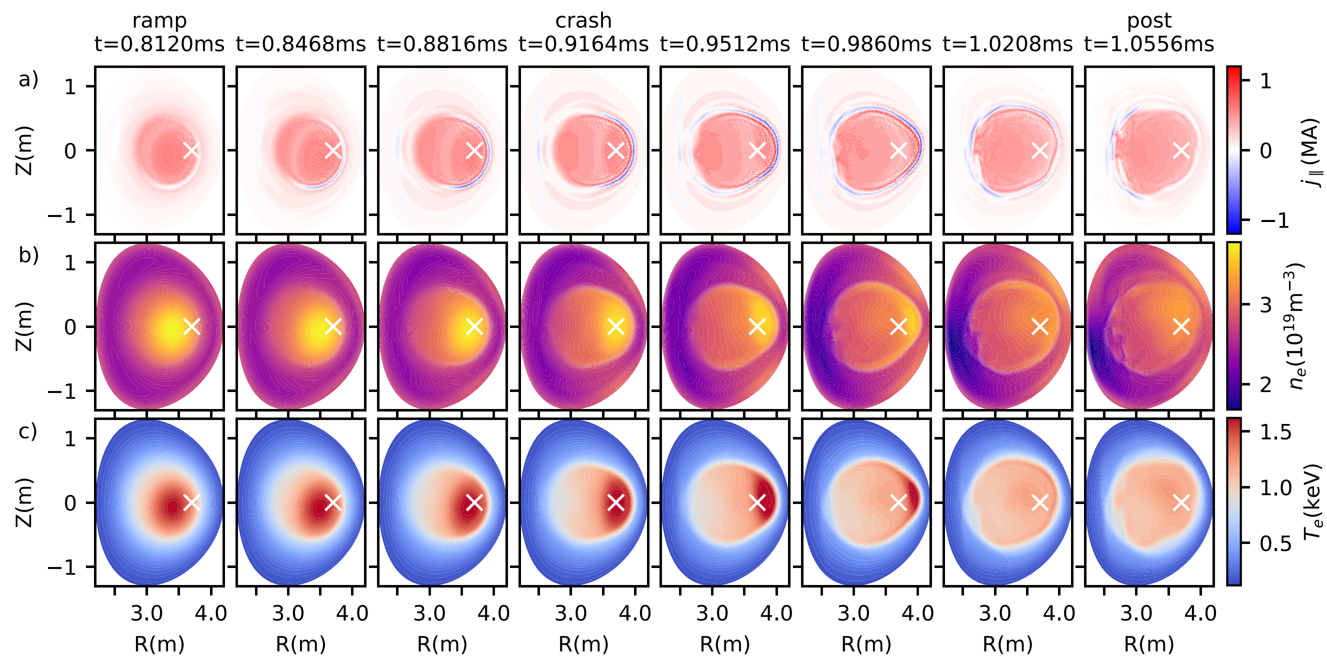

FIG. 5. 2D profiles taken during a sawtooth event for case 1: (a) $j_\parallel$, (b) n_e, and (c) T_e. The location of the inversion layer on the midplane is marked by a white cross.

taken as the distance that the magnetic axis has shifted from its initial location. We measure this quantity in the simulations from the core shift in the Poincaré surfaces, and we define ξ as normalized by r_1, the minor radius of the $q = 1$ surface. The oscillations of electron density and electron temperature, $\langle \delta n_e \rangle / \langle n_e \rangle$ and $\langle \delta T_e \rangle / \langle T_e \rangle$, are taken at $(R, Z) = (3.76, 0)$ m, where the $q = 1$ surface intersects with the midplane. They are normalized with their toroidal-averaged gradients at the moment ramp, $\langle \nabla n_e / n_e \rangle r_1$ and $\langle \nabla T_e / T_e \rangle r_1$. As is shown in Fig. 10, we find that both of them depend linearly on ξ,

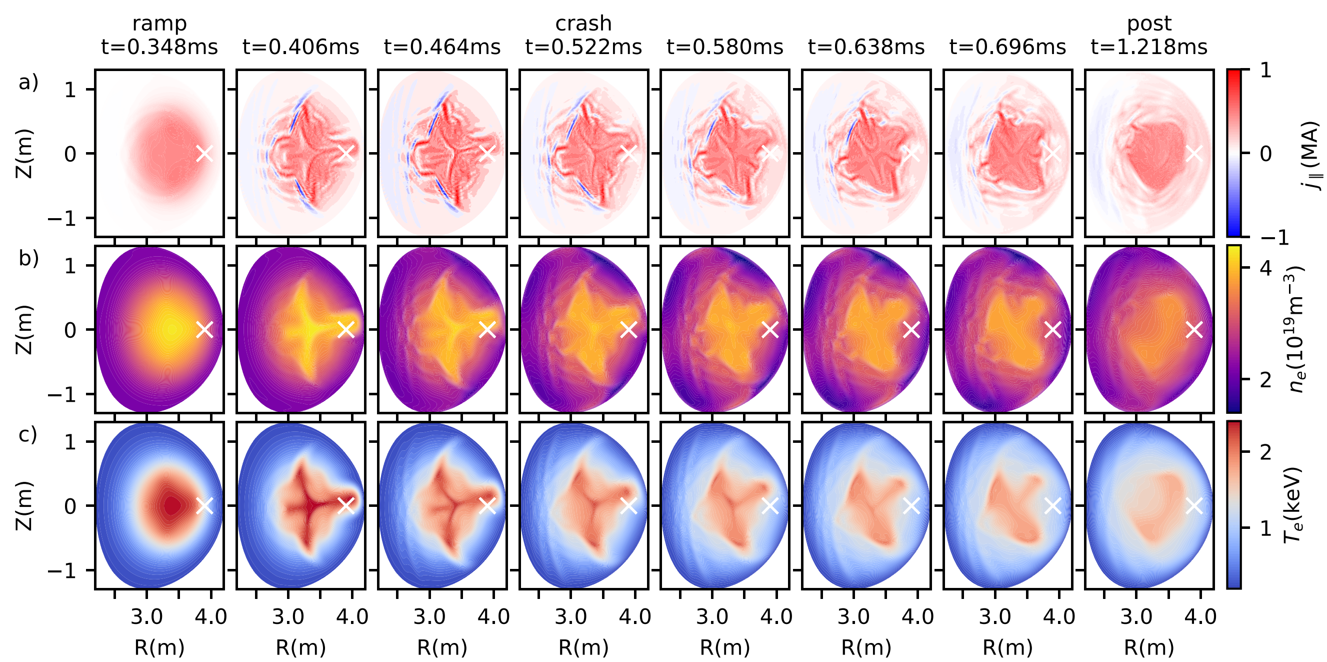

FIG. 6. 2D profiles taken during a sawtooth event for case 2: (a) $j_\parallel$, (b) n_e, and (c) T_e. The location of the inversion layer on the midplane is marked by a white cross.

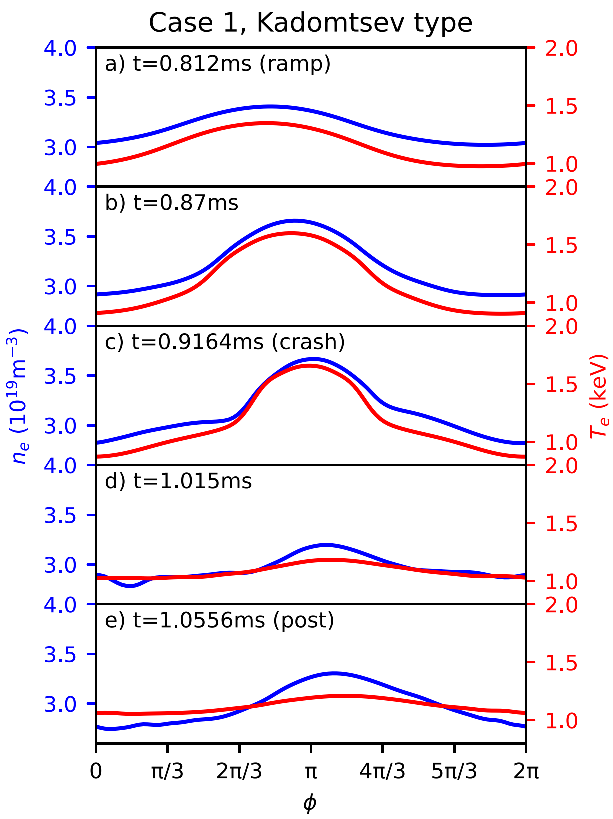

FIG. 7. Toroidal oscillations of n_e and T_e on the midplane near the inversion layer in the sawtooth of case 1. (a), (c), and (e) are taken at the time-points ramp, crash, and post and [(b) and (d)] are taken at the time-points in between.

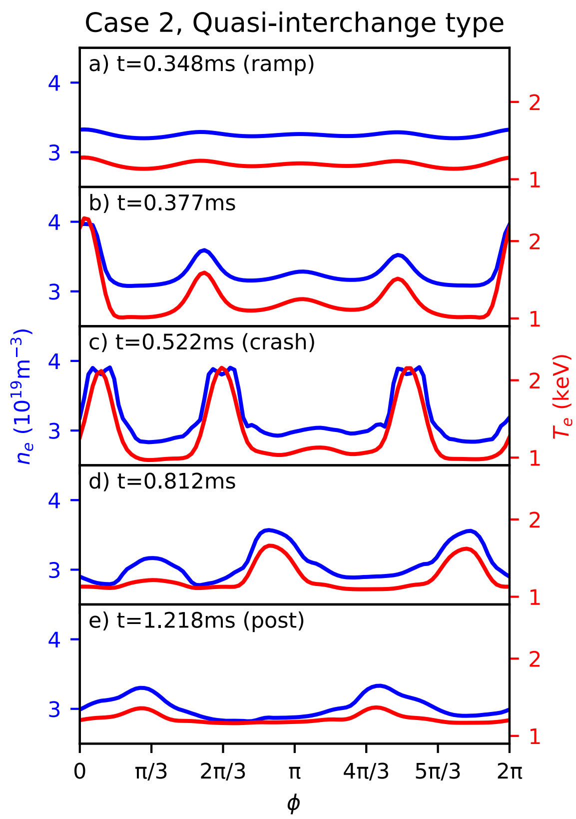

FIG. 8. Toroidal oscillations of n_e and T_e on the midplane near the inversion layer in the sawtooth of case 2. (a), (c), and (e) are taken at the time-points ramp, crash, and post and [(b) and (d)] are taken at the time-points in between.

$$\frac{\langle \delta n_e \rangle / \langle n_e \rangle}{\langle \nabla n_e / n_e \rangle r_1} \approx 0.4197\xi - 0.0275, \tag{2a}$$

$$\frac{\langle \delta T_e \rangle / \langle T_e \rangle}{\langle \nabla T_e / T_e \rangle r_1} \approx 0.4178\xi - 0.0228. \tag{2b}$$

The slopes are so close reinforces that the density and temperature evolve in phase.

With the integral form of Faraday's law,

$$\oint \mathbf{E} \cdot d\mathbf{l} = -\frac{d\Psi}{dt}, \tag{3}$$

we can calculate how much flux is reconnected during a sawtooth event by integrating the left hand side over time. We calculate the integral $\oint \mathbf{E} \cdot d\mathbf{l}$ numerically from simulation data using several toroidal planes, and we start the time integration when the island first appears. As is shown in Fig. 11, the amount of flux reconnected in the sawtooth event exhibits a good quadratic fit for ξ,

$$\Delta\Psi_{norm} \approx 0.0365\xi^2 + 0.0005\xi, \tag{4}$$

where $\Delta\Psi_{norm} = \Delta\Psi/(2\pi R r_1 B_p(q=1))$. This is not surprising because as the magnetic field lines inside the island are reconnected, the area of the island scales as the square of the core displacement.

With Eqs. (2) and (4), we can establish relations between the amount of reconnection and the oscillations of n_e and T_e near the $q = 1$ surface in a sawtooth event

$$\Delta\Psi_{norm} \approx 0.216(\delta n_e)^2_{norm} + 0.011(\delta n_e)_{norm}, \tag{5a}$$

$$\Delta\Psi_{norm} \approx 0.274(\delta T_e)^2_{norm} - 0.001(\delta T_e)_{norm}, \tag{5b}$$

where $(\delta n_e)_{norm}$ denotes $(\langle \delta n_e \rangle / \langle n_e \rangle)/\langle \nabla n_e / n_e \rangle r_1$, and $(\delta T_e)_{norm}$ denotes $(\langle \delta T_e \rangle / \langle T_e \rangle)/\langle \nabla T_e / T_e \rangle r_1$. The amount of reconnection is associated with the reconnection rate, so this relation quantifies reconnection via indirect diagnostics to study the fast timescale of the crash. In an experiment, given a $\delta n_e / n_e$ measured by BES, knowing the normalization factors ∇n_e, R, r_1, and $B_p(q=1)$, we will be able to estimate the reconnection rate $E_\parallel$. For example, with setups similar to the simulation, if $\delta n_e / n_e \sim 10\%$, then we can infer that $E_\parallel \sim 30\,(\mathrm{V\,m^{-1}})$. The exact coefficients may vary with specific plasma parameters in reality though. Samoylov *et al.*[16] have shown a relation between the reconnection rate and the displacement of the plasma core measured by ECEI in ASDEX Upgrade. This quantity is determined by the radial velocity of the plasma core, which they ascribe to the inflow velocity to the reconnection site. By contrast, our reconnection rate is obtained from

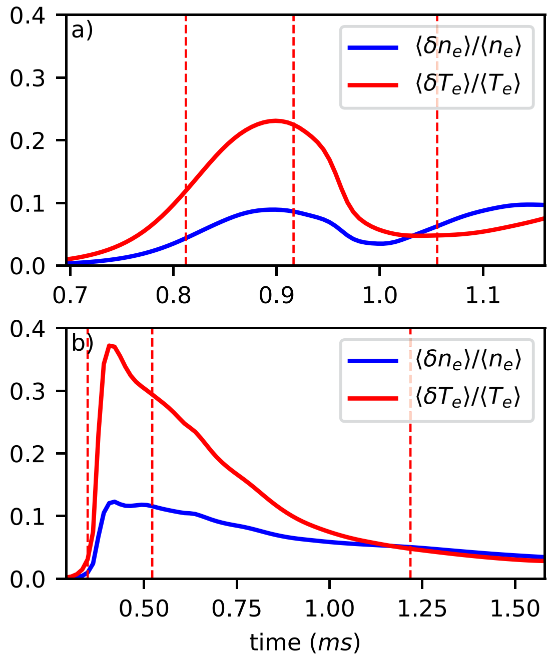

FIG. 9. The root mean square of the oscillation amplitude along the toroidal direction: (a) case 1, Kadomtsev type and (b) case 2, quasi-interchange type.

Faraday's law and directly quantifies how much magnetic field flux has been reconnected.

VI. DISCUSSIONS AND CONCLUSIONS

In this section, we first review and summarize our results and then comment on several aspects and open questions for this area. Here, we have studied the Kadomtsev and quasi-interchange sawtooth scenarios, both within 3D resistive MHD. First, we discuss

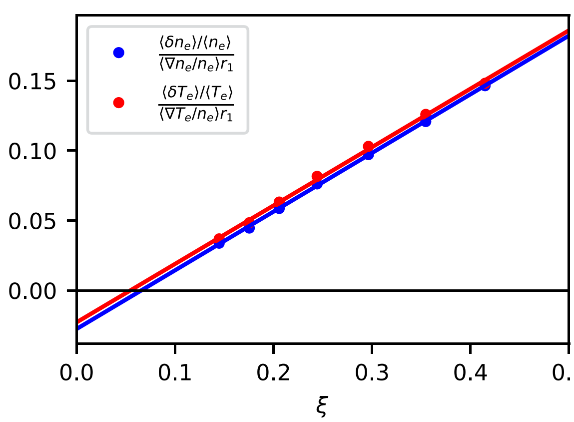

FIG. 10. Normalized oscillations of n_e (blue) and T_e (red) at the $q = 1$ surface on the midplane. The scattered dots are derived from the diagnostics and the lines are the linear fits.

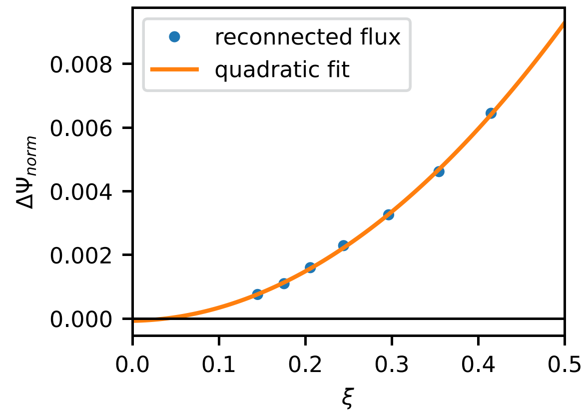

FIG. 11. Relation of reconnected flux to core kink amplitude. The scattered dots are derived from the diagnostics and the orange curve is a quadratic fit.

the broader set of parameters we have scanned, which support the main results that we have presented. Second, we discuss the connections of these results to other proposed sawtooth scenarios. Finally, we comment on the role of magnetic reconnection in the quasi-interchange case.

In this paper, we have studied two comparative sawtooth simulations. First of all, we have identified them as two different types of sawteeth. In case 1, q_0 starts from the initial value of 0.83 and is brought back to unity by the crash. The kinetic energy increases on a hybrid resistive/ideal timescale. The density and temperature profiles peak more strongly with the plasma heating and are flattened out rapidly as the crash occurs. A long thin current sheet appears during the crash, and the dominant (1, 1) island grows and replaces the original core. This behavior follows the predictions of the Kadomtsev model. In case 2, q_0 remains very close to unity through the whole process, and no single long current sheet forms during the crash. The kinetic energy grows on a faster ideal MHD timescale. Higher number modes dominate, but the configuration of the magnetic field does not change significantly, and the original core persists in case 2, which follows the quasi-interchange model.

Our analysis shows that for the Kadomtsev case, n_e and T_e are consistently dominated by a (1, 1) structure, and they always stay in phase. The correlation is a consequence of the hot core kinking outward. On the other hand, the quasi-interchange case is dominated first by a (4, 4) mode and later other high number modes, which are also reflected in the structures of n_e and T_e. Therefore, the spectral content of n_e and T_e can be used as a criterion to discriminate between the two types of sawtooth in future experiments. The toroidal oscillations of electron density and temperature local to the $q = 1$ surface, $\langle \delta n_e \rangle / \langle n_e \rangle$ and $\langle \delta T_e \rangle / \langle T_e \rangle$, are obtained using the simulation diagnostics data. The toroidal averaged density oscillation in n_e and T_e peak at the beginning of the crash, and they have large peak amplitude as reported from previous experiments. We find both cases have $(\langle \delta n_e \rangle / \langle n_e \rangle)_{max} \sim 10\%$, which is of similar level as the measurements of the BES on DIII-D by Bose *et al.*[18] Although $(\langle \delta T_e \rangle / \langle T_e \rangle)_{max}$ differs by case, showing ∼20% for the Kadomtsev case and ∼40% for the quasi-interchange case, this is still comparable to the measurements of the ECEI on ASDEX Upgrade by Samoylov *et al.*[23] Further study of the Kadomtsev case finds a quadratic relation between the amount of reconnection and the toroidal oscillations of n_e and T_e. This technique connects the newly developed measurement capabilities for n_e and T_e to the study of internal sawtooth behaviors.

While the main goal of this paper is the comparative study of two representative sawtooth scenarios, we have also conducted multiple supporting simulations with modified equilibria and simulation parameters to confirm the generality of the results. For the Kadomtsev case, by varying the initial q_0 between 0.7 and 0.9, we found that the overall qualitative behavior did not change, and in particular, all cases led to a (1, 1) mode driving magnetic reconnection. Second, we also scanned the initial plasma pressure (p_0) value. In this case, we observed that the flux surfaces stayed more organized with lower pressure, whereas high pressures led to more stochastization of the field after the crash. We also varied some parameters within the quasi-interchange scenario. In this case, slightly higher initial q_0 leads to less significant crash in T_e. In the simulations, the Lundquist number is lower than in reality but high enough to achieve a quasi-interchange type of sawtooth in case 2.

We next discuss how our results may relate to other sawtooth scenarios that have been proposed. In addition to the Kadomtsev model and the quasi-interchange model studied in this work, there have been other models addressing the tokamak sawtooth phenomenon. For example, Porcelli *et al.*[32] propose a heuristic model of incomplete sawtooth reconnection, where the poloidal symmetry is restored quickly before the reconnection completes due to the development of widespread magnetic turbulence. However, we did not enter this scenario in our simulations, and as far as we know, this model has never been demonstrated in a consistent nonlinear 3D MHD simulation.

Finally, while the role of reconnection has long been recognized as a crucial issue in the Kadomtsev reconnection scenario, its potential role in the quasi-interchange case is more subtle.[30] In the Kadomtsev scenario, the finite rate of reconnection in resistive MHD leads to a bottleneck in the evolution. The initial resistive instability also grows on a timescale that is a hybrid between the ideal and resistive timescales. These effects show a clear importance of resistive reconnection in controlling the dynamics in the Kadomtsev scenario. In the quasi-interchange scenario, by contrast, there is a collection of higher-order (m, n) modes, which grow and together drive stochastization of the field. The stochastization of the field and flux surface breakup requires some level of non-ideal electric field, and it is possible to associate this with reconnection. However, at present, it is not known if the reconnection will be a significant bottleneck to this process as it is for the Kadomtsev reconnection scenario. For example, the initial modes appear to grow on an ideal timescale (Fig. 3). Separately, and interestingly, Boozer[31] has pointed out that ideal MHD instabilities can cause flux surface breakup with vanishingly small resistivity. Future work, which analyzes the details of the magnetic field reconfiguration during the quasi-interchange crash and quantifies the nature of reconnection in this fully 3D system, could provide some valuable and fundamental insight for MHD.

ACKNOWLEDGMENTS

We are grateful to Andreas Kleiner, Brendan Lyons, and Chen Zhao for their technical support with the M3D-C1 code. This work was supported by the U.S. Department of Energy, Office of Fusion Energy and Sciences through the Frontier Science Program under Contract No. DE-AC0209CH11466.

TABLE II. Non-default parameters in the input file of M3D-C1 simulation for case 2.

Category	Variable	Value
Equilibrium	`itaylor`	1
	`eps`	1.0×10^{-8}
	`icsym`	1
	`xlim`	4.20
	`xlim2`	2.20
	`xmag`	3.2874
	`igs`	200
	`p0`	0.035
	`pi0`	0.0175
	`p1`	−0.5
	`pedge`	0.0015
	`expn`	0.2
	`q0`	0.975
	`tcuro`	0.8
	`tol_gs`	4.0×10^{-8}
Transport	`iresfunc`	4
	`eta_fac`	264
	`amu`	1.0×10^{-5}
	`kappa0`	1.75×10^{-6}
	`kappar`	5.0
	`denm`	1.0×10^{-5}
Hyper-diffusivity	`deex`	0.04
Normalization	`n0_norm`	4.0×10^{13}
Mesh	`nplanes`	36
Beam heating	`ibeam`	1
	`beam_x`	3.3
	`beam_rate`	1.6×10^{23}
	`beam_dr`	0.3
	`beam_fracpar`	0.2
Current control	`vloop`	-1.0×10^{-5}
	`tcur`	0.8
	`control_type`	1
	`control_p`	-1.0×10^{-3}
	`control_i`	-1.0×10^{-6}
Density control	`ipellet`	2
	`pellet_rate`	3.0×10^{-5}
	`n_control_type`	1
	`n_control_p`	1.0×10^{-5}
	`n_control_i`	1.0×10^{-8}
	`n_target`	56.54

The United States Government retains a non-exclusive, paid-up, irrevocable, world-wide license to publish or reproduce the published form of this manuscript, or allow others to do so, for United States Government purpose.

AUTHOR DECLARATIONS

Conflict of Interest

The authors have no conflicts to disclose.

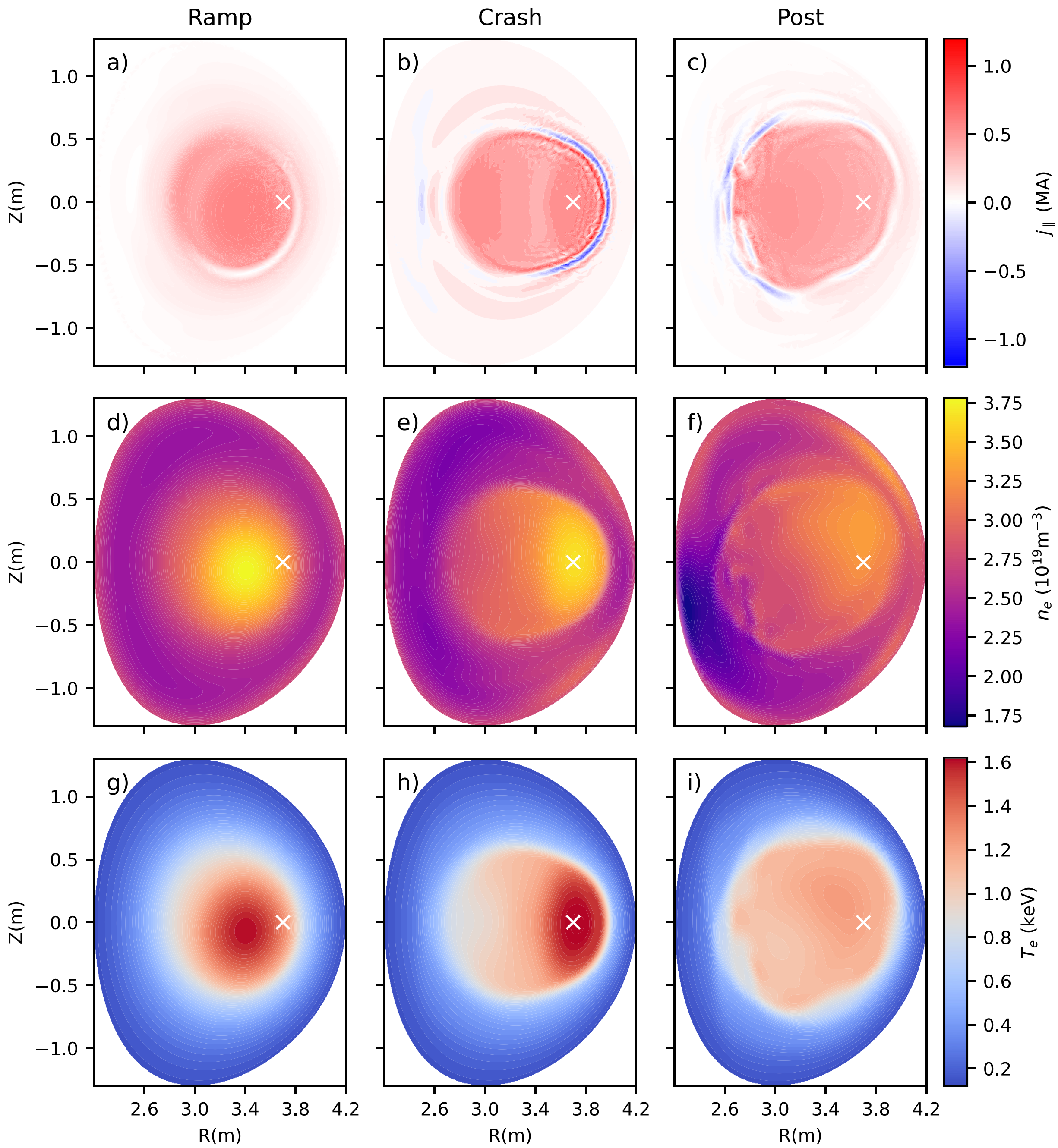

FIG. 12. Zoom-in view of 2D profiles taken at the time-points ramp, crash, and post for case 1: (a)–(c) $j_\parallel$; (d)–(f) n_e; and (g)–(i) T_e. The location of the inversion layer on the mid-plane is marked by a white cross.

Author Contributions

D. Liu: Data curation (lead); Formal analysis (lead); Investigation (lead); Methodology (lead); Validation (lead); Visualization (lead); Writing – original draft (lead); Writing – review & editing (lead). **W. Fox:** Conceptualization (lead); Data curation (equal); Formal analysis (supporting); Funding acquisition (lead); Investigation (equal); Methodology (equal); Project administration (lead); Resources (lead); Supervision (lead); Validation (equal); Visualization (supporting); Writing – review & editing (equal). **S. Bose:** Investigation (supporting); Methodology (supporting); Supervision (supporting); Visualization (supporting); Writing – review & editing (supporting). **H. Ji:** Investigation (supporting); Supervision (supporting); Writing – review & editing (supporting).

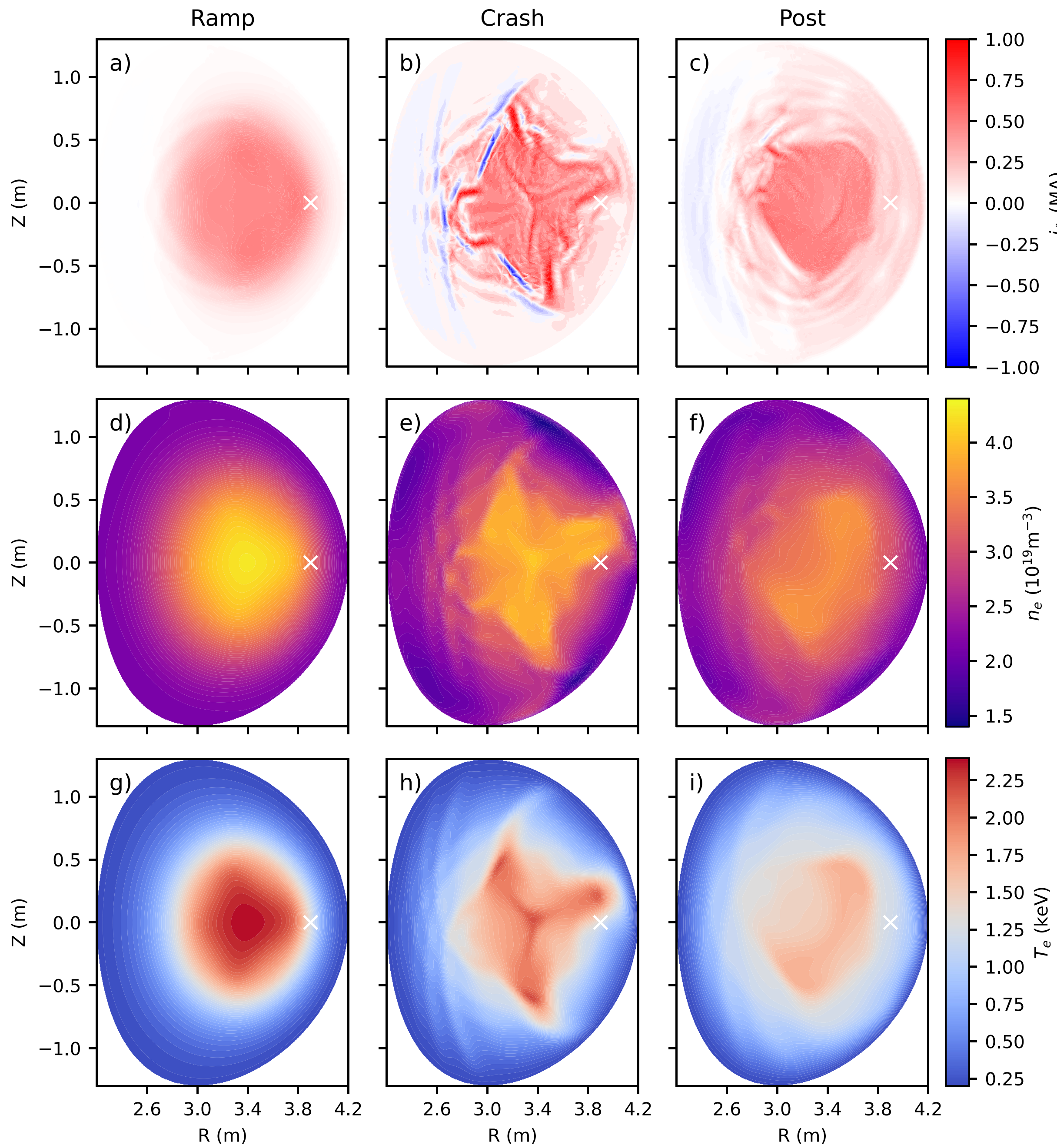

FIG. 13. Zoom-in view of 2D profiles taken at the time-points ramp, crash, and post for case 2: (a)–(c) $j_\parallel$; (d)–(f) n_e; and (g)–(i) T_e. The location of the inversion layer on the mid-plane is marked by a white cross.

S. Jardin: Data curation (equal); Investigation (supporting); Methodology (supporting); Resources (lead); Software (lead); Validation (equal); Visualization (supporting); Writing – review & editing (supporting). **N. Ferraro:** Investigation (supporting); Methodology (supporting); Software (lead); Writing – review & editing (supporting).

DATA AVAILABILITY

The input parameters of the simulations presented in this paper are given in Appendix A.

APPENDIX A: DETAILS ON THE SIMULATION SETUPS

Non-default parameters in the input file of M3D-C1 simulation are listed for case 2 in Table II, and case 1 can be set up with the substitution in Table I.

APPENDIX B: ZOOM-IN VIEW OF FIGS. 5 AND 6

To show the 2D structures of $j_{\|}$, n_e, and T_e with more details, we append the zoom-in view of Figs. 5 and 6 at the three characteristic time-points ramp, crash, and post with Figs. 12 and 13.

REFERENCES

[1] R. J. Hastie, Astrophys. Space Sci. **256**, 177 (1997).
[2] I. T. Chapman, Plasma Phys. Controlled Fusion **53**, 013001 (2011).
[3] B. B. Kadomtsev, Sov. Tech. Phys. Lett. **1**, 5 (1975) [Pis'ma Zh. Tekh. Fiz. **1**, 710–715 (1975)]; see https://www.osti.gov/biblio/7147025.
[4] M. Yamada, F. M. Levinton, N. Pomphrey, R. Budny, J. Manickam, and Y. Nagayama, Phys. Plasmas **1**, 3269 (1994).
[5] R. G. Kleva, J. F. Drake, and F. L. Waelbroeck, Phys. Plasmas **2**, 23 (1995).
[6] A. Bhattacharjee, Y.-M. Huang, H. Yang, and B. Rogers, Phys. Plasmas **16**, 112102 (2009).
[7] J. A. Wesson, Plasma Phys. Controlled Fusion **28**, 243–248 (1986).
[8] S. C. Jardin, I. Krebs, and N. Ferraro, Phys. Plasmas **27**, 032509 (2020).
[9] S. C. Jardin, N. Ferraro, and I. Krebs, Phys. Rev. Lett. **115**, 215001 (2015).
[10] W. Fox, F. Sciortino, A. V. Stechow, J. Jara-Almonte, J. Yoo, H. Ji, and M. Yamada, Phys. Rev. Lett. **118**, 125002 (2017).
[11] R. J. Goldston, Phys. Fluids **21**, 2346 (1978).
[12] H. Soltwisch, Rev. Sci. Instrum. **59**, 1599 (1988).
[13] F. M. Levinton, Rev. Sci. Instrum. **63**, 5157 (1992).
[14] H. K. Park, M. J. Choi, M. Kim, M. Kim, J. Lee, D. Lee, W. Lee, and G. Yun, Rev. Mod. Plasma Phys. **6**, 18 (2022).
[15] T. Munsat, H. Park, I. Classen, C. Domier, A. Donné, N. Luhmann, E. Mazzucato, M. van de Pol, and TEXTOR Team, Nucl. Fusion **47**, L31 (2007).
[16] O. Samoylov, V. Igochine, Q. Yu, H. Zohm, and ASDEX Upgrade Team, Nucl. Fusion **62**, 074002 (2022).
[17] H. K. Park, A. J. H. Donné, N. C. Luhmann, I. G. J. Classen, C. W. Domier, E. Mazzucato, T. Munsat, M. J. van de Pol, Z. Xia, and TEXTOR Team, Phys. Rev. Lett. **96**, 195004 (2006).
[18] S. Bose, W. Fox, D. Liu, Z. Yan, G. McKee, A. Goodman, and H. Ji, Rev. Sci. Instrum. **93**, 093521 (2022).
[19] S. Jardin, J. Breslau, and N. Ferraro, J. Comput. Phys. **226**, 2146 (2007).
[20] M. T. Beidler, P. A. Cassak, S. C. Jardin, and N. M. Ferraro, Plasma Phys. Controlled Fusion **59**, 025007 (2017).
[21] J. A. Breslau, S. C. Jardin, and W. Park, Phys. Plasmas **14**, 056105 (2007).
[22] J. A. Breslau, C. R. Sovinec, and S. C. Jardin, Commun. Comput. Phys. **4**, 647 (2008); see http://global-sci.org/intro/article_detail/cicp/7809.html.
[23] O. Samoylov, V. Igochine, A. Stegmeir, and H. Zohm, J. Plasma Phys. **88**, 905880116 (2022).
[24] S. C. Jardin, N. Ferraro, J. Breslau, and J. Chen, Comput. Sci. Discovery **5**, 014002 (2012).
[25] S. von Goeler, W. Stodiek, and N. Sauthoff, Phys. Rev. Lett. **33**, 1201 (1974).
[26] A. W. Edwards, D. J. Campbell, W. W. Engelhardt, H. U. Fahrbach, R. D. Gill, R. S. Granetz, S. Tsuji, B. J. D. Tubbing, A. Weller, J. Wesson, and D. Zasche, Phys. Rev. Lett. **57**, 210 (1986).
[27] V. S. Udintsev, M. Ottaviani, P. Maget, G. Giruzzi, J.-L. Ségui, T. Aniel, J. F. Artaud, F. Clairet, M. Goniche, G. T. Hoang, G. T. A. Huysmans, F. Imbeaux, E. Joffrin, D. Mazon, A. L. Pecquet, R. Sabot, A. Sirinelli, L. Vermare, T. S. Team, A. Krämer-Flecken, H. R. Koslowski, T. Team, A. J. H. Donné, F. C. Schüller, C. W. Domier, N. C. Luhmann, and S. V. Mirnov, Plasma Phys. Controlled Fusion **47**, 1111 (2005).
[28] V. Igochine, O. Dumbrajs, H. Zohm, A. Flaws, and ASDEX Upgrade Team, Nucl. Fusion **47**, 23 (2007).
[29] Y. Nam, J. Ko, G. Choe, Y. Bae, M. Choi, W. Lee, G. Yun, S. Jardin, and H. Park, Nucl. Fusion **58**, 066009 (2018).
[30] V. Igochine, Phys. Plasmas **30**, 120502 (2023).
[31] A. H. Boozer, Phys. Plasmas **30**, 062113 (2023).
[32] F. Porcelli, D. Boucher, and M. N. Rosenbluth, Plasma Phys. Controlled Fusion **38**, 2163 (1996).